

PREPARATION AND EFFECTS OF TEMPERATURE ON NANOCRYSTALLINE ITO PARTICLES SYNTHESIZED BY CO-PRECIPITATION WITH DIFFERENT SnO_2 CONTENT

ZM Hanafi, FF Hammad and AM Youssef
Inorganic Chemistry Department, National Research Centre, Dokki, Cairo, Egypt

ABSTRACT

Indium tin oxide (ITO) nanopowders of different compositions (In: Sn = 90:10, 70:30 and 50:50) were prepared by heat treatment (300–950°C) of mixed hydroxides of In(III) and Sn(IV). The hydroxides were obtained by the reaction of aqueous NH_3 mixed with aqueous solutions of $\text{In}(\text{NO}_3)_3$ and SnCl_4 . Two kinds of nanocrystalline indium tin oxide (ITO) powders with different crystal structures (rhombohedral and cubic) were prepared and examined. During sintering the rhombohedral ITO was transformed to cubic around 950 °C. The lattice parameter was calculated from XRD analysis is 10.104 Å and the particle size range is 19.9 - 23.1 nm.

Keywords: Indium tin oxide (ITO), nanopowders, XRD analysis, the lattice parameter, the particle size

INTRODUCTION

Indium tin oxide (ITO) is the most widely used transparent conductive oxides (TCOs) for its high conductivity and excellent transparency (Zhan *et al.*, 2007). This metal oxide can be promised for various applications due to its interesting optical, electronic and surface properties. ITO has been widely used in the microelectronic applications, including transparent heating elements for aircraft and car windows (Molnar *et al.*, 1999) solar cells (Herrero and Guillen, 2002) heat reflecting mirrors for glass windows (Xu *et al.*, 2004) gas sensors (Luff *et al.*, 1997) photovoltaic devices (Bellingham *et al.*, 1991) chemistry as a photo catalyst (Tsch'ope *et al.*, 1996) and in a variety of electro-optical devices, such as liquid-crystal flat panel displays (Osaza *et al.*, 1994). Especially, co-precipitation process has been used in many fields of advanced ceramics because the product purity and homogeneity have the possibility to control the physical properties and particles shapes. On the other hand, the route is operated easily and requires few expensive apparatuses and instruments. There are many process parameters, which can affect the properties and shapes of ITO powder, including reactant pH, stoichiometric ratio, amount of added tin chloride, synthesis temperature and calcination ambience (Li *et al.*, 2006).

This work mainly deals with the effects of synthesis temperature and calcinations temperature on morphology and phase structure of ITO particles. The sintering characteristics of nanocrystalline ITO powders with different crystal structures, cubic and rhombohedral, were

examined. During sintering, phase transformation occurred in the ITO powder and the effect of phase transformation on densification of nanocrystalline ITO powder was examined.

MATERIALS AND METHODS

Indium tin oxide (ITO) nanopowders of different compositions (In: Sn = 90:10, 70:30 and 50:50) were prepared by wet-chemical co-precipitation processing technique (Pramanik and Biswas, 2002) from the starting materials, aqueous $\text{In}(\text{NO}_3)_3$ and $\text{SnCl}_4 \cdot 5\text{H}_2\text{O}$. The mixture was diluted with water and the resulting solution was stirred magnetically for 2h at 65°C. Concentrated aqueous NH_3 was added dropwise to the above mixture and the pH of the above solution was maintained in the range 7.0-7.5. The mixture was stirred for additional 5h at an ambient temperature till a gel of hydrated indium tin oxide appeared. The precipitate was collected by filtration under vacuum, washed with water. A white powder solid was obtained. The samples were heated at 300°C, under air atmosphere. Structural analysis was carried out using X-ray diffractograms provided with computer controlled X-ray diffractometer [formally made by Daino Corporation, USA] equipped with Co radiation $\text{CoK}\alpha$ ($\lambda = 1.79026 \text{ \AA}$). The scanning range was 20 – 80 (2 θ) with step size of 0.02° (2 θ) and counting time of 3 s/step. Quartz was used as the standard material to correct for the instrumental broadening. Refinement by Fullprof program Rodrigues-Carvajal (2004) was used for lattice parameter determination and Winfit program (Krumn, 1994) for size/strain analysis. TEM images were taken with a JEOL model 1230 transmission electron microscope.

*Corresponding author email: fdw_hammad@yahoo.com

RESULTS AND DISCUSSION

Figures 1, 2, 3 show the X-ray diffraction patterns of indium tin oxide nanopowder at different temperatures and different compositions (In: Sn =90:10, 70:30 and 50:50 wt.%). It is clear that there is no any diffracted line for pure In_2O_3 or any phases corresponding to tin or to other tin compounds showing that the Sn was in solution in the In_2O_3 .

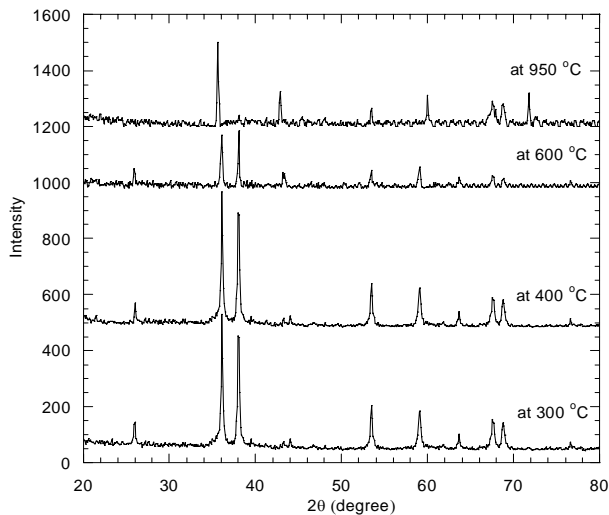


Fig. 1. X-ray diffraction patterns of (In: Sn = 90:10 wt.%) samples heated at different temperatures.

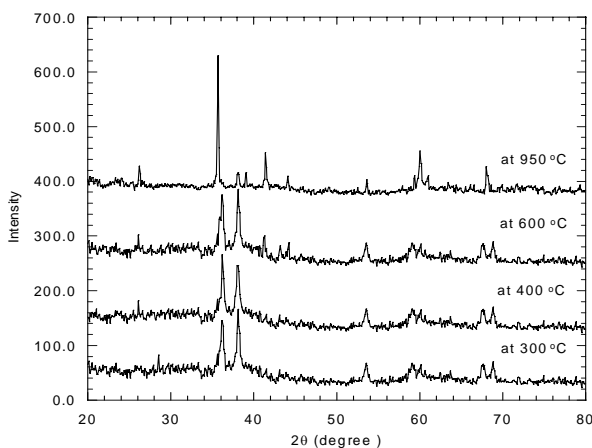


Fig. 2. X-ray diffraction patterns of (In: Sn = 70:30 wt.%) samples heated at different temperatures

It is found that the samples with the composition (In: Sn=90:10 and 70:30) prepared at 300 and 400°C possess pure rhombohedral structure since the peak (104) corresponding to rhombohedral In_2O_3 (White and Keramida, 1972). At 600°C this sample possesses a mixture of rhombohedral-cubic structure with sharp diffraction peaks. The deconvoluted x-ray peaks of (222) and (104)

corresponding to cubic (Hamberg and Granqvist, 1986) and rhombohedral (White and Keramida, 1972) respectively confirmed the results obtained by (Kim *et al.*, 2002). It is clear that rhombohedral-cubic phase transformation process occurred near 600°C, in the case of the samples, which were initially composed of mostly rhombohedra. Rhombohedral structure disappeared and cubic structure appeared when the sample was sintered at 950°C. This can be attributed to the fact that all Sn is soluble in In_2O_3 and it forms a single phase of ITO.

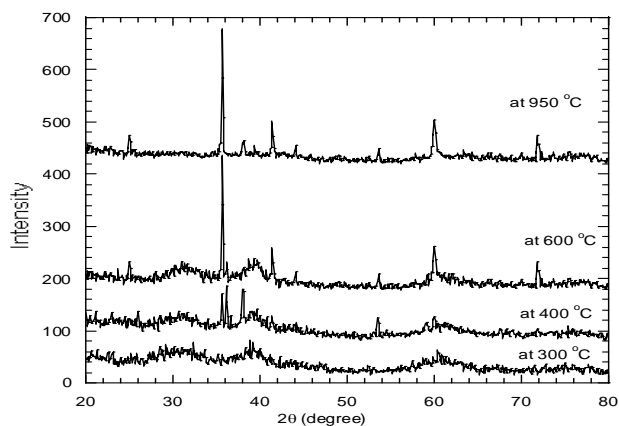


Fig. 3. X-ray diffraction patterns of (In/ Sn = 50:50 wt.%) samples heated at different temperatures.

Alam and Cameron (2000) show the XRD spectrum of an air-annealed 10 wt.% Sn-doped ITO annealed at 600°C are polycrystalline with a cubic bixbyite structure with no preferred orientation. Kim *et al.* (2006) prepared nanocrystalline ITO powder with different Sn content from 0 to 12 wt.% by a co-precipitation method after heat treatment for 1h at 600, 1100, 1350 and 1550°C as a function of the Sn content. After 48h of aging time, a cubic ITO phase was produced as a major phase. Osaza *et al.* (1994) found that the phase transformation proceeded even at low temperature of 800°C. However, hundreds of hours of annealing at 800°C were necessary for a complete phase transformation.

Figure 3 shows the X-ray diffraction patterns of the synthesized indium tin oxide (In: Sn= 50:50 wt.%) heated at different temperatures. No peaks ascribed to the phase of tin compounds are observed, indicating that all tin ions came into the lattice of In_2O_3 to substitute for indium ions. It is shown very poor crystallinity at 300°C but at 400°C and 600°C, a mixture of cubic and rhombohedral phases appear and single phase of cubic In_2O_3 appeared at 950°C. This may be due to the increasing of the crystallinity of nanopowder. Udawatte and Yanagisawa (2001) obtained the same results for 300°C hydrothermally synthesized In_2O_3 particles. The peaks of the sample synthesized at 400°C are stronger than at

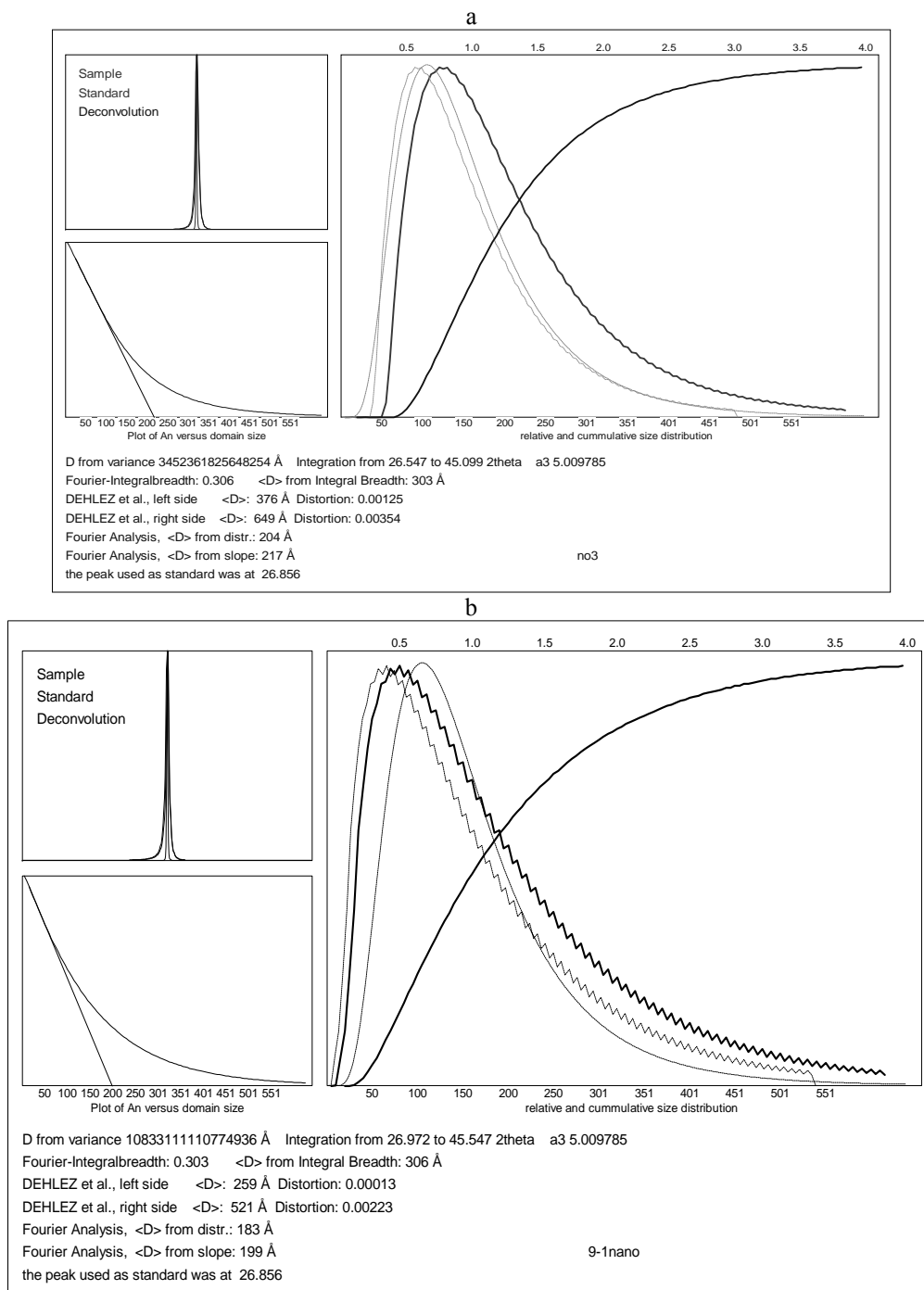


Fig. 4. Profile fitting of (222) Bragg reflection peak and Plot of normalized Fourier coefficients versus domain Size (dotted strain line is tangent to the straight part of the curve) of (a) Pure In_2O_3 and (b) In: Sn = 90:10 wt.% nanopowder.

300°C showing that increasing temperature greatly improves the particle crystallinity, and this confirms the substantially amorphous as shown in figure 3. This phenomenon can be explained as follows, In^{3+} and Sn^{4+} exhibit similar chemical properties, they combine with OH^- to form $\text{In}(\text{OH})_3$ and $\text{Sn}(\text{OH})_4$ in solution firstly.

Under the thermal conditions, these $\text{In}(\text{OH})_3$ and $\text{Sn}(\text{OH})_4$ partly lose water in the molecule and transform into InOOH phase (Udawatte and Yanagisawa, 2001). In other words, the $\text{In}(\text{OH})_3$ and $\text{Sn}(\text{OH})_4$ provide feeds for this transformation. When the thermal temperature is too low, this driving force is weak and the obtained particles were

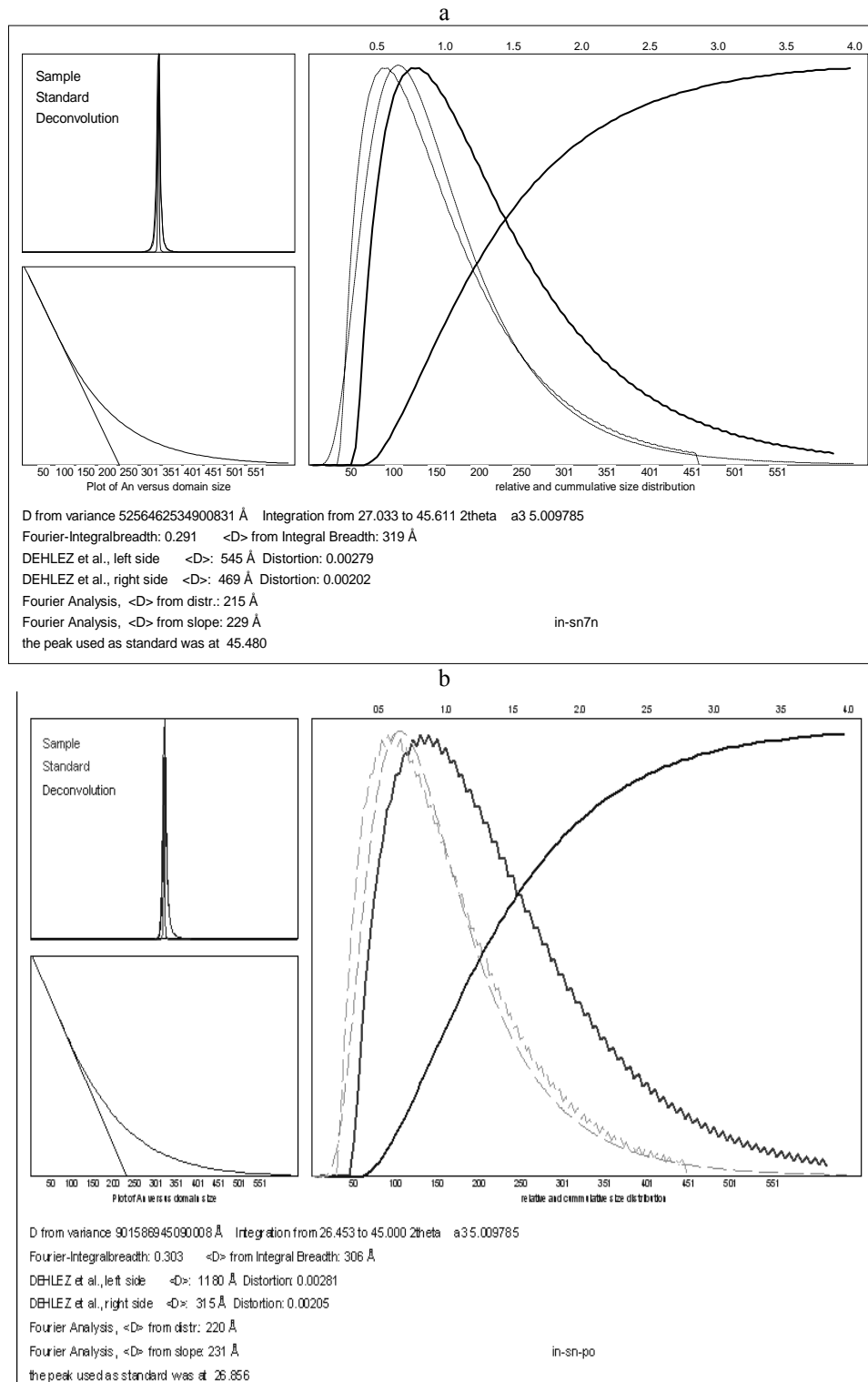


Fig. 5. Profile fitting of (222) Bragg reflection peak and Plot of normalized Fourier coefficients versus domain Size (dotted strain line is tangent to the straight part of the curve) of (a) In: Sn = 70:30 wt.% nanopowder and (b) In: Sn = 50:50 wt.% nanopowder.

mainly amorphous. Increasing the temperature promotes this transformation and a very thin with a finer diameter

was formed with high crystallinity.

Table 1. Values of lattice constant (a,c) and Unit cell volume (V) for (In: Sn= 90:10 wt.%) nanopowder sample.

Sample	At 300 °C	At 400 °C	At 600 °C	At 950 °C
Cubic Phase	-	-	-	a= 10.103
	-	-	-	V= 1031.1
Rhombohedral phase	a= 5.487	a= 5.480	a= 5.478	-
	c=14.542	c=14.526	c=14.498	-
	V= 379.2	V= 377.8	V= 376.83	-

Table 2. Values of lattice constant (a,c) and Unit cell volume (V) for (In: Sn= 70:30 wt.%) nanopowder sample.

Sample	At 300 °C	At 400 °C	At 600 °C	At 950 °C
Cubic Phase	-	-	a= 10.117	a= 10.113
	-	-	V= 1035.1	V= 1034.5
Rhombohedral phase	a= 5.485	a= 5.480	a= 5.473	-
	c=14.506	c=14.482	c=14.518	-
	V= 378.1	V= 377.5	V= 376.6	-

Table 3. Values of lattice constant (a,c) and Unit cell volume (V) for (In: Sn= 50:50 wt.%) nanopowder sample.

Sample	At 300 °C	At 400 °C	At 600 °C	At 950 °C
Cubic Phase	-	a= 10.125	a= 10.122	a= 10.118
	-	V= 1038	V= 1037	V= 1035.7
Rhombohedral phase	-	a= 5.489	a= 5.479	-
	-	c=14.519	c=14.506	-
	-	V= 378.9	V= 377.1	-

Table 4. The particle size and micro-strain of In₂O₃ pure and that doped with different concentration of SnO₂.

Sample	In ₂ O ₃	In:Sn=90:10	In:Sn = 70:30	In:Sn = 50:50
Crystallite size (nm)	21.7	19.9	22.9	23.1
Internal strain (%)	0.00479	0.00236	0.00481	0.00486

It is very interesting to note that the white precursor hydrous oxide is amorphous to X-rays while on calcination at 400°C, some changes occur in its colour than the characteristics pale yellow colour (Devi *et al.*, 2002) of In₂O₃. It is evident that with increasing the calcination temperature, the intensity of the peak increases significantly along with a reduction in the peak half width indicating the growth of ITO particles with the calcination temperature.

The locations and relative intensities of all peaks were almost the same as those of In₂O₃ with cubic structure except that all peak locations shifted little towards smaller diffraction angles. The shifts of the peak locations should

be attributed to the formation of ITO solid solution by doping with Sn⁴⁺ at In³⁺ site in the In₂O₃ lattice, for higher effective charge of Sn⁴⁺ compared to In³⁺ caused higher repulsion forces (Chen *et al.*, 2004).

The lattice parameter and Unit cell volume for nanoparticles was calculated and tabulated in tables 1, 2 and 3 for cubic and rhombahedral phases. The values obtained are in good agreement with those obtained by different authors (Devi *et al.*, 2002; Shimada *et al.*, 1988). It is difficult to observe any clear tendencies. However, all ITO samples exhibit a larger lattice parameter than that of pure In₂O₃, a =10.104 Å, giving additional evidence for the incorporation of Sn⁴⁺ into the indium oxide lattice

and, thus, for the formation of solid solutions. The observed increase in the lattice parameter is consistent with the data reported in the literature. A decrease in the unit cell volume as the tin content increases is due to the smaller ionic radius of Sn^{4+} (0.71 Å) compared to that of In^{3+} (0.81 Å) because of the fact that the Sn^{4+} ions have the choice between two different indium sites. Depending on whether they occupy the In1 or In2 positions the influence on the oxygen stoichiometry, the lattice parameters, and the bond lengths is different. All the output of the winfit program are shown in the figures 4-5.

True profile of the (222) reflection at $2\theta \approx 35\text{-}36^\circ$ corrected from the instrumental broadening, was used for the determination of crystalline size and lattice strain, especially because no overlapping with any other reflection. Any smoothing procedure may lead to distortion of the original peak profile and may introduce significant errors into the data (Howard and Preston, 1989).

The crystalline size and internal residual strain were determined by the one-order (single line) method. The profile fitting of the (222) Bragg reflection of In_2O_3 pure and ITO with different concentrations of SnO_2 are given and the normalized Fourier coefficients $A(n)$ are plotted versus the domain size $L (= n d_{222})$ in figures 4 and 5. From the intercept of the straight part of the curve with the X-axis an average value of the crystalline size and strain was obtained approach that implemented in WinFit. Size and strain from profile analysis are given in table 4.

It is clear that the effect of particle size as a function of concentration is not a systematic relation to the value of the particle size. It decreases in 10 wt.% SnO_2 and then increases as a function of dopant concentration as shown in table 4.

Discussing the effect of dopant concentration on micro-strain $|\epsilon|$, it is clear that the value decreases at 10 wt. % and then increases. This may be due to the fact that the ionic radii for the different ions leading to this difference of behavior.

CONCLUSION

In conclusion, the dominant factor in line broadening may be due to the presence of strain due to addition of different concentrations besides the change in lattice parameter values which resulted from created defects.

REFERENCES

Alam, MJ. and Cameron, DC. 2000. Optical and electrical properties of transparent conductive ITO thin films deposited by sol-gel process. *Thin Solid Films*. 377-378:455-459.

Bellingham, JR., Mackenzie, AP. and Philips, WA. 1991. Precise measurements of oxygen content: Oxygen vacancies in transparent conducting indium oxide films. *Appl. Phys. Lett.* 58:2506-2511.

Chen, SG., Li, CH., Xiong, WH., Liu, LM. and Wang, H. 2004. Preparation of indium-tin oxide (ITO) aciculae by a novel concentration-precipitation and post-calcination method. *Materials Letters*. 58:294-298.

Devi, PS., Chatterjee, M. and Ganguli, D. 2002. Indium tin oxide nano-particles through an emulsion technique. *Materials Letters*. 55:205-210.

Hamberg, I. and Granqvist, CG. 1986. Evaporated Sn-doped In_2O_3 films: Basic optical properties and applications to energy-efficient windows. *J. Appl. Phys.* 60:123-129.

Herrero, J. and Guillen, C. 2002. Transparent films on polymers for photovoltaic applications. *Vacuum* 67:611-616.

Howard, SA. and Preston, D. 1989. Profile fitting of powder diffraction patterns. *Reviews in Mineralogy and Geochemistry*. 20:217-275.

Kim, BC., Kim, SM., Lee, JH. and Kim, JJ. 2002. Effect of Phase Transformation on the Densification of Coprecipitated Nanocrystalline Indium Tin Oxide Powders. *J. Am. Ceram. Soc.* 85 (8):2083-2088.

Kim, SM., Seo, KH., Lee, JH., Kim, JJ., Lee, HY. and Lee, JS. 2006. Preparation and sintering of nanocrystalline ITO powders with different SnO_2 content. *Journal of the European Ceramic Society* 26:73-80.

Krumn, S. 1994. XIII Conference on Clay Mineralogy and Petrology, Praha, Acta Universitate Carolinae. 38:254.

Li, ST., Qiao, XL., Chen, JG., Wang, HS., Jia, F. and Qiu, XL. 2006. Effects of temperature on indium tin oxide particles synthesized by co-precipitation. *Journal of Crystal Growth*. 289:151-156.

Luff, BJ., Wilkinson, JS. and Perrone, G. 1997. Indium tin oxide overlayers waveguides for sensor applications. *Appl. Opt.* 36: 7066-7072.

Molnar, K., Mohacsy, T., Varga, P., Vazsonyi, E. and Barsony, I. 1999. Characterization of ITO/porous silicon LED structures *Lumin.* 80:91-97.

Osaza, K., Ye, T. and Aoyagi, Y. 1994. Deposition of thin indium oxide film and its application to selective epitaxy for *in situ* processing. *Thin Solid Films*. 246:58-64.

Pramanik, NC. and Biswas, PK. 2002. Development of nano indium tin oxide (ITO) grains by alkaline hydrolysis of In(III) and Sn(IV) salts. *Bull. Mater. Sci.* 5(6):505-507.

- Rodrigues-Carvajal, J. 2004. Reference Guide of Fullprip Program, Laboratory Leon Brillouin [CEA-CNRS], version July, 2004.
- Shimada, S., Sato, I., Kodaira, K. and Matsushita, T. 1988. Growth of Pure and Tin-Doped Indium Oxide Crystals and Their Electrical Properties. *J. Electrochem. Soc.* 135(12):3165-3166.
- Tschöpe, A., Ying, JY. and Tuller, HL. 1996. Catalytic redox activity and electrical conductivity of nanocrystalline non-stoichiometric cerium oxide. *Sens. Actuators. B* 31:111-114.
- Udawatte, CP. and Yanagisawa, K. 2001. Fabrication of Low-Porosity Indium Tin Oxide Ceramics in Air from Hydrothermally Prepared Powder. *J. Am. Ceram. Soc.* 84 (1):251-253.
- Xu, CY., Liu, L., Legenski, SE., Ning, D. and Taya, M. 2004. Switchable window based on electrochromic polymers. *J. Mater. Res.* 19:2072-2080.
- White, WB. and Keramida, VG. 1972. Vibrational spectra of oxides with the C-type rare earth oxide structure. *Spectrochim. Acta. A* 28:501-509.
- Zhang, J., Gao, L. and Chen, M. 2007. A novel solvothermal method to synthesize one-dimensional chains of indium tin oxide nanoparticles. *Materials Letters.* 61:2671-2674.